11th International Symposium on Turbulence and Shear Flow Phenomena (TSFP11)
Southampton, UK, July 30 to August 2, 2019

# TURBULENT-TURBULENT TRANSITION OF A TRANSIENT THREE-DIMENSIONAL CHANNEL FLOW

**Shuisheng He**
Department of Mechanical Engineering
University of Sheffield
Sheffield S1 3JD, UK
Email: s.he@sheffield.ac.uk

**Adrián Lozano-Durán**
Center for Turbulence Research
Stanford University
450 Serra Mall, Stanford, CA 94305, USA
Email: adrianld@stanford.edu

**Jundi He**
Department of Mechanical Engineering
University of Sheffield
Sheffield S1 3JD, UK
Email: jhe21@sheffield.ac.uk

**Minjeong Cho**
Center for Turbulence Research
Stanford University
450 Serra Mall, Stanford, CA 94305, USA
Email: minjeong@stanford.edu

## ABSTRACT

A transient three-dimensional turbulent flow is investigated using direct numerical simulation (DNS). The flow is initiated by subjecting a statistically stationary turbulent channel flow to a constant transverse pressure gradient while maintaining the streamwise pressure gradient unchanged. It is shown that this transient three-dimensional flow can be described as a transition between two turbulent states characterized by the development of a buffeted laminar boundary layer in an initial turbulent environment followed by transition to turbulence.

## INTRODUCTION

Three-dimensional turbulent boundary layers (3DTBL) are commonplace in aerodynamic applications. Despite intensive studies, there still remain intriguing fundamental questions regarding the flow structures and turbulence to be answered. Moin *et al.* (1990) and more recently Giometto *et al.* (2017) studied a three-dimensional boundary layer resulted from subjecting an initially statistically stationary turbulent 2D channel flow to a transverse pressure gradient. This relatively simple configuration contains many interesting flow physics that are common in more complex 3DTBLs.

Moin *et al.* (1990) numerically demonstrated the reduction in Reynolds stresses and the lag between the directions of the shear stress vector and the mean velocity gradient observed in complex 3DTBLs. They explained the decay of turbulence in the transient process to be a chain of events that is largely related to the suppression of a pressure-strain mechanism. In a closely related work, Sendstad & Moin (1991) investigated the flow structure changes of this 3D flow.

Giometto *et al.* (2017) focused on the scaling of the 3DTBLs and the performance of wall-modelling techniques for large-eddy simulation (LES) for this non-equilibrium turbulent flow. They significantly extended the range of flow conditions covered by Moin *et al.* (1990) and performed DNS for three Reynolds numbers: $Re_\tau$ = 934, 546 and 186 and one pressure gradient for each of the first two cases ($dP/dz = 10\ dP/dx$; $dP/dz = 40\ dP/dx$) and various pressure gradients for the lowest Re, i.e., $dP/dz = 1 \sim 125\ dP/dx$. They demonstrated that the turbulent shear stress near the wall scales well in the inner units for different $Re_\tau$ but the same $(dP/dz)^+$ where $+$ denotes wall units, whereas in the core region, the results collapse in the outer units for different $Re_\tau$ but the same ratio of friction velocities in the spanwise and streamwise directions $(w_\tau/u_\tau)$.

Note that both of the above studies showed that the initial response of the mean flow is well described by the laminar flow solution and that the turbulence intensity increases after an initial period when it is suppressed. In particular, Giometto *et al.* (2017) obtained results for a longer time and observed that the turbulent shear stress is significantly increased after an initial reduction ($Re_\tau = 546$).

Among the large body of literature in 3DTBLs (not discussed here due to space limitation), it is worth noting the work by Howard & Sandham (2001) who carried out an investigation of a channel flow in which the 3-D flow is caused by suddenly moving the top and bottom walls in the spanwise direction at a constant speed. They associated the reduction in turbulence to the destruction of the lifting side of the vortices. In parallel, Kannepalli (2000) reported an LES of a 3D boundary layer resulting from a section of the wall (some distance away from the leading edge) moving in the transverse direction and observed the straining of the near-wall turbulence structures.

In present study, the 3DTBL is analyzed from a new perspective following the approach and theory recently established in a series of studies of a transient channel flow subjected to a streamwise pressure gradient (He & Seddighi, 2013, 2015; Mathur *et al.*, 2018). The transient flow in these studies resulted from an increase of the mass flow rate (in the flow direction) to an initially stationary turbulent flow in a channel or a pipe. It was demonstrated that this transient flow is characterized by a laminar-turbulent transition. In response to the rapid increase of flow rate, the flow does not progressively evolve from the initial turbulent structure to a new one, but rather undergoes a process involving three

distinct phases. These are pre-transition, transition and fully turbulence that resembles the three regions of the boundary layer bypass transition: the buffeted laminar flow, the intermittent flow, and the fully turbulent flow regions.

## METHODOLOGY

A series of direct numerical simulations of fully developed incompressible planar channel flows similar to those of Giometto *et al.* (2017) have been carried out, with a focus on the initial transient response after the application of a sudden transverse pressure gradient. Reynolds number $Re_\tau$ = 186 is defined in terms of the channel half-height $h^*$, the friction velocity $u^*_{\tau 0}$ and the kinematic viscosity $\nu^*$. Dimensional variables are shown as $()^*$, and the subscript "0" indicates the value at $t$=0. Wall units + are defined in terms of $u^*_{\tau 0}$ and $\nu^*$. Outer units, shown with no sub- or superscripts, are obtained by normalization using the initial bulk velocity ($U^*_{b0}$) and $h^*$ except time, which is scaled by $u^*_{\tau 0}$ and $h^*$. The streamwise, wall-normal and spanwise directions are represented by $x$, $y$ and $z$, respectively, and the corresponding velocities are $u$, $v$ and $w$. Velocities averaged in the homogeneous directions and then ensemble-averaged over several runs are denoted by $U$, $V$, and $W$, and fluctuating quantities are signified by $()'$. The three-dimensional transient flow is initialized from a fully developed equilibrium planar channel flow at the corresponding Reynolds number by suddenly applying a transverse pressure gradient, which is maintained unchanged throughout the transient flow simulation. The streamwise pressure gradient is maintained at its initial value. Simulations have been carried out for a set of spanwise pressure gradients.

The incompressible Navier-Stokes equations are integrated by a fully staggered second-order centered finite difference method in space. Time advancement is performed via a third-order accurate Runge-Kutta method, and the system of equations is solved via an operator splitting approach. The code has been validated in previous studies in turbulent channel flows (Bae *et al.*, 2018) and flat-plate boundary layers (Lozano-Durán *et al.*, 2018).

The computational domain is $L_x{}^* = 4\pi h^*$ and $L_z{}^* = 2\pi h^*$ in the streamwise and spanwise directions, respectively. At the time prior to applying the spanwise pressure gradient, the grid resolutions are $\Delta x^+ = 9.1$, $\Delta z^+ = 4.5$, $\Delta y^+_{min} = 0.3$ and $\Delta y^+_{max} = 6.4$. The results are denoted following the convection dpdzX where X is the spanwise to streamwise pressure gradient ratio. Simulations for two streamwise accelerated flows have also been carried out, denoted as dpdx10 and dpdx30.

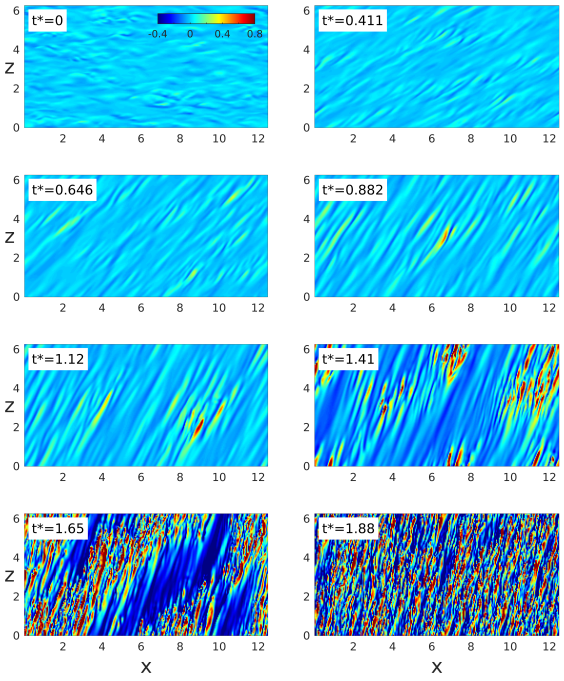


Figure 1. Spanwise fluctuating velocity in a xz plane with $y^{+0}$=3.76 in case dpdz30.

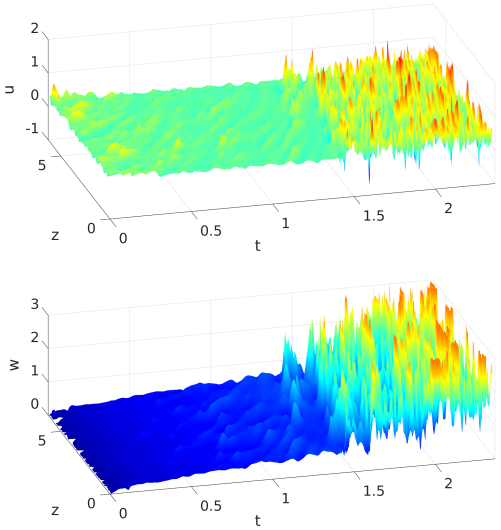


Figure 2. Variation of the streamwise (left) and spanwise (right) velocities along a horizontal line across the channel at $y^+ = 2.2$, case dpdz30.

## RESULT AND DISCUSSION

### The observation of transition

The response of the instantaneous flow following the imposition of a constant transverse pressure gradient is visualized in Figures 1. Figure 1 shows contours, at a number of times, of the instantaneous spanwise fluctuating velocity in a wall-parallel plane at $y^{+0} = 3.76$ for case dpdz30. The first observation is the formation of new tilted streaks up to $t(= t^* u^*_{\tau 0}/h^*) = 1.41$, and the increase in their angles with time. The latter is clearly due to the rotation of the total mean flow with time under the influence of the transverse pressure gradient. However, the streaks do not actually rotate but instead streaks of a certain angle formed at earlier times are weakened at later times and replaced by new streaks formed at an increased angle. This process continues in time, leading to streaks formed at only some discrete angles. The second observation is the formation of turbulent spots, which first appear at $t = 1.12$, and multiple spots are clearly observed at $t = 1.41$. At later times, these spots grow and connect to each other, covering larger areas of the flow. Finally, the entire domain is populated by new turbulence at $t = 1.88$.

The above observations suggest that the transient three-dimensional turbulent flow of concern here is characterized by a buffeted laminar boundary layer developed in the span-

wise direction, followed by a bypass transition, even though the initial flow is already turbulent. This process resembles the laminar-turbulent bypass transition of a boundary layer over a flat plate subjected to a relatively high free-stream turbulence (Jacobs & Durbin, 2001; Matsubara & Alfredsson, 2001). The transitional framework proposed here is a radically new interpretation of the transient three-dimensional turbulent flow and expands the theory established in He & Seddighi (2013, 2015) to a more complex 3D flow scenario.

Additional evidence is shown in Figure 2, which displays the time development of the instantaneous velocities $u$ and $w$ along a horizontal line across the span of the channel. Initially, both velocities remain largely unchanged until about $t \approx 1.1$, when abrupt increases occur in both of them, but which fade away shortly thereafter. This response is likely caused by turbulent spots crossing the probing line. Later at $t = 1.3$, rapid variations occur again in both $u$ and $w$ which are sustained in time. At this stage, the sudden change in the amplitude is also accompanied by discontinuous changes in the time and spatial scales (in the horizontal and vertical abscissae, respectively) - both scales undergo a sudden reduction, suggesting that the flow switches from an initial lower Reynolds number state to one of a higher Reynolds number state.

## The time developing, transverse flow, boundary layer

Following the application of the transverse pressure gradient, the flow in the entire channel accelerates uniformly in the spanwise direction as a plug flow, except in the vicinity of the wall where no-slip boundary condition applies because of viscosity. In this region, the velocity of the fluid reduces rapidly from the bulk value to zero at the wall. Consequently, a thin boundary layer is formed, which grows away from the wall with time. To study the behavior of this boundary layer, we compare it with the corresponding laminar flow caused by the same flow acceleration. This is an extended Stokes first problem whereby the mass flow rate increases with time in a non-uniform way, rather than a step change as in the classical Stokes problem. The solution of this problem provides the time-developing velocity as follows (Schlichting & Gersten, 2016)

$$W(y,t) = \int_0^t W_b'(\tau) erfc\left(\frac{y}{2\sqrt{\nu(t-\tau)}}\right) d\tau, \qquad (1)$$

where erfc is the complementary error function and $W_b'(t)$ the bulk flow acceleration.

Figure 3 shows a comparison between the transient boundary layer obtained from the DNS and Stokes laminar solution. The two profiles agree closely during the pre-transitional phase until around $t$=1.2, after which they deviate from each other. The DNS result assumes a profile that is representative of turbulent flow. The time when the deviation occurs corresponds roughly to the onset of transition shown in Figures 1 to 2. During the initial pre-transitional period, the stream velocity remains largely unchanged (not shown).

Figures 4(a, b) show the development of the friction coefficient in the streamwise and spanwise directions, defined as $C_{fx} = \tau^*_{w,x}/2{U_b}^{*2}$, $C_{fz} = \tau^*_{w,z}/2{W_b}^{*2}$, respectively. The onset of transition is marked in each case using a triangle. These are defined here with the minimum $C_{fx}$, consistent with the time when turbulent spots are generated in Figures 1 to 2. The friction factor $C_{fx}$ is more appropriate for this purpose than $C_{fz}$, since the variation of the former is mostly influenced by the transient evolution of the turbulence flow without the influence of the development of the development of an additional boundary layer, whereas the latter is also influenced by the growth of the new boundary layer. The friction coefficient for the extended Stokes solution is given by

$$C_f = \frac{1}{2W_b^2}\int_0^t W_b'(\tau)\sqrt{\frac{\nu}{\pi(t-\tau)}}d\tau. \qquad (2)$$

Figure 4(b) indicates that $C_{fz}$ from the DNS agrees closely with that from the Stokes solutions up to the point of onset of transition, supporting our earlier statement. The figure also shows that $C_{fx}$ decreases during pre-transition, which can be related to the initial laminarization to be shown later and also reported in previous studies (Moin *et al.*, 1990). The stronger the acceleration, the stronger the reduction in $C_{fx}$, which trend is reversed after the transition. The friction factor $C_{fz}$ also shows a progressively decreasing trend in the pre-transitional phase, but this is due to the growth of the new boundary layer. This trend is also reversed following the transition in dpdz30 and dpdz100, but the change in the case of dpdz10 is rather subtle.

Figure 5 shows the (equivalent) transitional Reynolds number ($Re_{cr}$) versus the "freestream" turbulence intensity ($Tu_0$), which are defined as

$$Re_{cr} = \frac{{x^*}_{cr} {W^*}_{b,cr}}{\nu^*} \text{ and } Tu_0 = \frac{\underset{y}{max}({u^*}'_{rms,0})}{{W^*}_{b,cr}}, \qquad (3)$$

where ${x_{cr}}^* = \int_0^{t^*_{cr}} W_b^* t^* dt^*$, $t^*_{cr}$ is the time at the onset of transition and $W^*_{b,cr}$ is the spanwise bulk velocity at $t^*_{cr}$. In bypass transition, $Re_{cr} = C(Tu_0)^n$ and n=2. Figure 5 shows that $Re_{cr}$ and $Tu_0$ appear to roughly follow this power law relationship, even though the index is likely to be different from "2". More extensive data are needed to confirm this relationship.

## Transition mechanisms and energy growth

Two potential transition mechanisms may occur in this three-dimensional flow: (i) bypass transition due to transient growth of the disturbances existing in the initial flow (Jacobs & Durbin, 2001; Matsubara & Alfredsson, 2001) and (ii) cross flow instability due to an inflectional velocity profile resulting from the application of the transverse pressure gradient (Saric *et al.*, 2003; Bippes, 1999; Schrader *et al.*, 2010).

After the application of the transverse pressure gradient, the main flow starts turning in the spanwise direction. The flow, however, rotates at different rates at different wall distances due to the effect of viscosity, which leads to the so-called cross flow. We use the direction of the velocity in the channel center to represent the principal flow ($U_P$), and the flow in the perpendicular direction to represent the cross flow ($W_P$). As shown in Figure 6(a), the flow increases relatively slowly initially, but it speeds up in the second half of

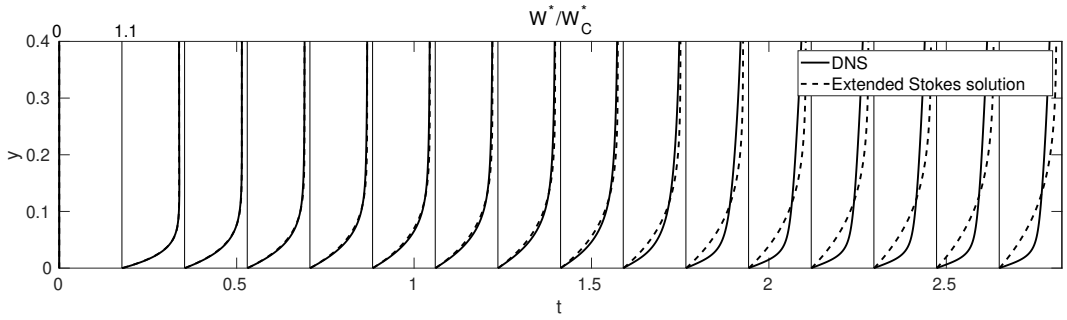


Figure 3. Spanwise velocity profile development in dpdz30 and comparison with the solution of extended Stokes first problem for an equivalent laminar acceleration. $W_c^*$ is the centerline velocity.

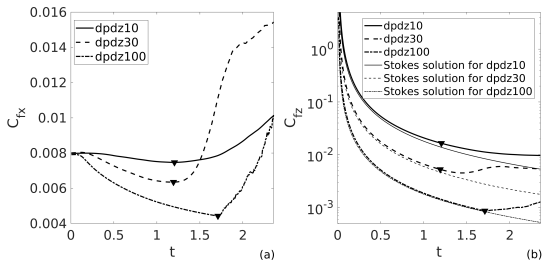


Figure 4. Friction coefficient in the streamwise (a) and spanwise (b) directions.

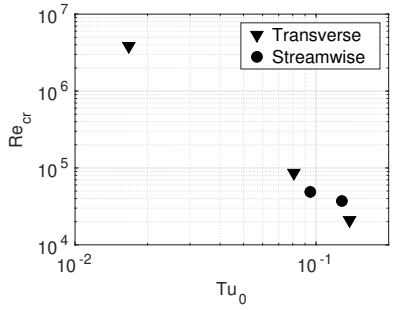


Figure 5. Critical Reynolds number versus freestream turbulence intensity.

the pre-transition period reaching a level that is more than double its initial value at $t$=1.2. In contrast, the cross flow (Figure 6(b)) is relatively strong shortly after start of the flow transient, at about half of the peak value at an earlier time of 0.2; both the amplitude and the extent further increase slightly until $t$ = 0.5, after which the cross flow appears to be largely unchanged until transition. The angle of the main flow changes continuously with time, as does the angle of the cross flow. Hence, even though the cross flow shown above remains largely unchanged during $t = 0.5 - 1.2$ in Figure 6(b), the actual velocity in the absolute coordinate undergoes a sustained change.

Cross flow instability can be investigated by studying the profiles of the directional velocity, i.e. the velocity projection on a vertical plane at an angle to the x-z plane (Bippes, 1999). The most unstable profiles are likely to be the active cause for transition. In the present case, the directional velocities vary with time. Such velocities are shown in Figure 7 for a number of times. Some velocities in the pre-transition phase clearly show inflectional point within the boundary layer region.

Next, we study the energy growth of the disturbances. Figure 9(a) shows the increase of the maximum streamwise fluctuating velocity with time. The increase of $\langle w'w' \rangle$ in dpdz10 and dpdz30 is largely linear in this semi-logarithmic plot in the pre-transitional period after an initial lag, implying that the energy growth is exponential during most part of the pre-transitional phase. Even though ordinarily, exponential growth can be associated with crossflow instability, whereas transient (algebraic) growth may lead to bypass transition (Andersson *et al.*, 1999; Luchini, 2000), no conclusion can be drawn here since the transverse flow itself increases with time in this flow. The response of $\langle w'w' \rangle$ in dpdz100 is, however, significantly different. It appears to exhibit a two-stage development, a rapid response followed by a slower stage. Figure 9(b) shows that during the pre-transition period, the peak value of $\langle u'u' \rangle$ drops significantly. In fact, as shown in Figure 9(c), the turbulence kinetic energy integrated over the channel height decreases in the initial stage of the pre-transition period ($t < 0.8$ for dpdz30, for example). It recovers at later times, and by the onset of transition, the energy is largely similar to that of the initial flow.

The variation of the disturbance energy observed above can be associated with the formation, destruction and regeneration of streaks with increasing angles to the initial flow shown in Figure 1, which implies a reduction in $\langle u'u' \rangle$ but an increase in $\langle w'w' \rangle$. The detailed variations of profiles of $\langle u'u' \rangle$ and $\langle w'w' \rangle$ are shown in Figure 8. In the pre-transition phase $\langle u'u' \rangle$ reduces near the wall, whereas $\langle w'w' \rangle$ increases. The new peak of $\langle w'w' \rangle$ appears to be at the same elevation as that of the $\langle u'u' \rangle$ of the initial flow, indicating that the new streaks are at a similar height as the initial ones. Some time after the onset of transition ($t = 1.5$), the peak of $\langle w'w' \rangle$ moves significantly closer to the wall consistent with the new turbulence. It might be useful to study the energy growth in the direction of the principal flow. Such information is shown in Figure 8(c). The energy reduces in the first part of the pre-transition, reaching a level much lower than the initial one. In the second part of the pre-transition, energy increases with time but only reaches its initial values at the time of onset of transition. This apparent reduction is largely due to the rotation of the principal flow and the lag of the growth of the disturbance in response.

It is interesting to compare the energy growth in the 3D (dpdz) and 2D (dpdx) transient flows. As Figure 9(a) indi-

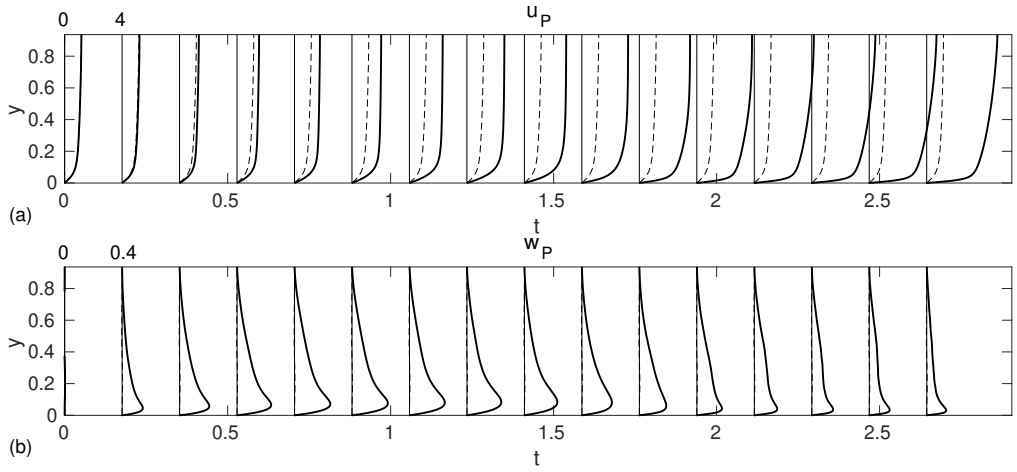


Figure 6. Development of the velocity profiles (a) along the centerline velocity direction $U_P$ (principal flow) and (b) perpendicular to it $W_P$ (cross flow) in case dpdz30. Dashed lines: initial flow, solid lines: profiles at t.

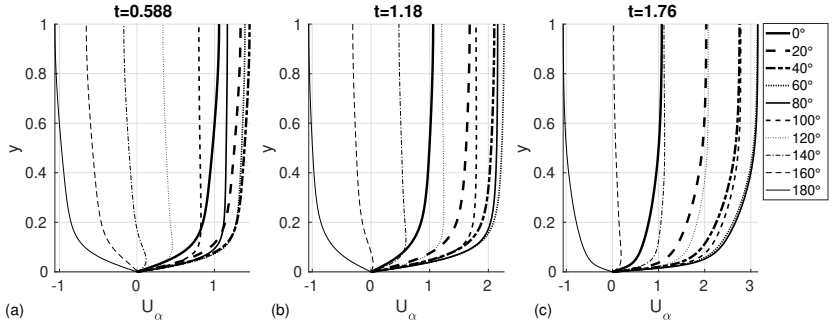


Figure 7. Directional velocity profiles at several time instants.

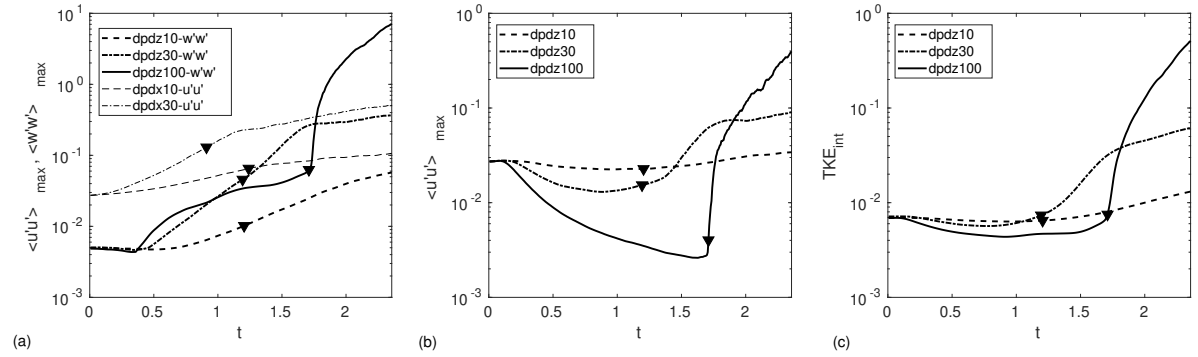


Figure 8. Energy growth in (a) the direction of flow acceleration, (b) direction perpendicular to it and (c) turbulence kinetic energy integrated over the channel height.

cates, the disturbance energy at the onset of transition in dpdx cases is significantly higher than that in the 3D flows. However, the rates of increase in the former cases are actually lower than those in the latter cases.

## CONCLUSIONS

A new interpretation of the transient three-dimensional turbulent boundary layer has been established. The transient response of the three-dimensional flow resulting from an imposition of a transverse pressure gradient on an initial 2D turbulent flow is shown to be characterized by spontaneous transition, even though the initial flow is already turbulent. The equivalent transitional Reynolds number is approximately related to freestream turbulence through a power law. Both cross flow and bypass (streaks) instabilities have been observed, but it not yet established in this study which one of these mechanisms causes the breakdown of the boundary layer. The dominant mechanism may be different in different transient cases, but this hypothesis is still

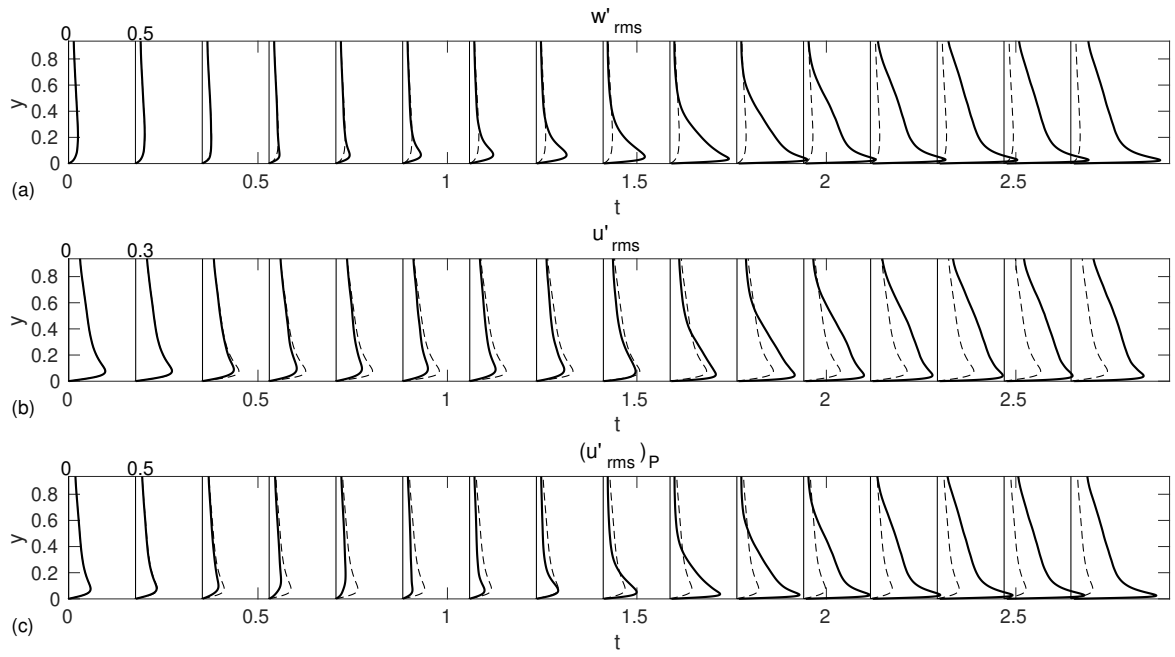


Figure 9. Development of the r.m.s. of the turbulent fluctuating velocities in (a) spanwise, (b) streamwise and (c) principal flow (centerline velocity) directions in case dpdz30. (Dashed lines: initial profiles at $t = 0$; solid lines: profiles at time $t$).

to be investigated.

## ACKNOWLEDGMENT

This investigation was funded by ONR under Grant #N00014-16-S-BA10. The authors acknowledge the computational resources granted by the Certainty cluster at CTR.

## REFERENCES

ANDERSSON, P., MARTIN, B. & DAN S, H. 1999 Optimal disturbances and bypass transition in boundary layers. *Phys. Fluids.* **11** (1), 134–150.

BAE, H. J., LOZANO-DURÁN, A., BOSE, S. T. & MOIN, P. 2018 Turbulence intensities in large-eddy simulation of wall-bounded flows. *Phys. Rev. Fluids* **3** (1), 1–11.

BIPPES, H. 1999 Basic experiments on transition in three-dimensional boundary layers dominated by crossflow instability. *Prog. Aerosp. Sci.* **35** (4), 363–412.

GIOMETTO, B. M. G., PARK, G. I. & MOIN, P. 2017 Three-dimensional transient channel flow at moderate Reynolds numbers: Analysis and wall modeling. *Annual Research Briefs*, Center for Turbulence Research, Stanford University, pp. 193–205.

HE, S. & SEDDIGHI, M. 2013 Turbulence in transient channel flow. *J. Fluid Mech.* **715**, 60–102.

HE, S. & SEDDIGHI, M. 2015 Transition of transient channel flow after a change in Reynolds number. *J. Fluid Mech.* **764**, 395–427.

HOWARD, R. J. A. & SANDHAM, N. D. 2001 Simulation and modelling of a skewed turbulent channel flow. *Flow Turbul. Combust.* **65** (1), 83–109.

JACOBS, R. G. & DURBIN, P. A. 2001 Simulations of bypass transition. *J. Fluid Mech.* **428**, 185–212.

KANNEPALLI, U. P. 2000 Large-eddy simulation of a three-dimensional shear-driven turbulent boundary layer. *J. Fluid Mech.* **423**, 175–203.

LOZANO-DURÁN, A., HACK, M. J. & MOIN, P. 2018 Modeling boundary-layer transition in direct and large-eddy simulations using parabolized stability equations. *Phys. Rev. Fluids* **3** (2), 1–16.

LUCHINI, P. 2000 Reynolds-number-independent instability of the boundary layer over a flat surface: optimal perturbations. *J. Fluid Mech.* **404**, 289–309.

MATHUR, A., GORJI, S., HE, S., SEDDIGHI, M., VARDY, A. E., O'DONOGHUE, T. & POKRAJAC, D. 2018 Temporal acceleration of a turbulent channel flow. *J. Fluid Mech.* **835**, 471–490.

MATSUBARA, M. & ALFREDSSON, P. H. 2001 Disturbance growth in boundary layers subjected to free-stream turbulence. *J. Fluid Mech.* **430**, 149–168.

MOIN, P., SHIH, T. H., DRIVER, D. & MANSOUR, N. N. 1990 Direct numerical simulation of a three-dimensional turbulent boundary layer. *Phys. Fluids.* **2** (10), 1846–1853.

SARIC, W. S., REED, H. L. & WHITE, E. B. 2003 Stability and transition of three-dimensional boundary layers. *Annu. Rev. Fluid Mech.* **35** (1), 413–440.

SCHLICHTING, H. & GERSTEN, K. 2016 *Boundary-layer theory*. Springer.

SCHRADER, L. U., AMIN, S. & BRANDT, L. 2010 Transition to turbulence in the boundary layer over a smooth and rough swept plate exposed to free-stream turbulence. *J. Fluid Mech.* **646**, 297–325.

SENDSTAD, O. & MOIN, P. 1991 On the mechanics of 3-D turbulent boundary layers. In *Symposium on Turbulent Shear Flows, 8 th, Munich, Federal Republic of Germany*, pp. 5–4.